Supporting Information for "The zonal patterns in late Quaternary tropical South American precipitation"

T. Kukla[1,2], M. J. Winnick[3], M. M. Laguë[4,5], Z. Xia[3,6]

[1]Department of Geosciences, Colorado State University, Fort Collins, CO, USA

[2]Department of Geological Sciences, Stanford University, Stanford, CA, USA

[3]Department of Geosciences, University of Massachusetts Amherst, Amherst, MA, USA

[4]University of Saskatchewan Coldwater Lab, Canmore, Alberta, Canada

[5]Department of Atmospheric Sciences, University of Utah, Salt Lake City, UT, USA

[6]Key laboratory of Geogrpahical Processes and Ecological Security in Changbai Mountains, Ministry of Education, School of Geographical Sciences, Northeast Normal University, Changchun, China

Contents of this file

Text S1: Quantifying moisture recycling connectivity between eastern, central, and western records

The first goal of the paper is to interpret past rainfall patterns from the spatial isotope gradient (negative $\Delta\delta^{18}O$ indicates decreasing $\delta^{18}O$ moving inland), rather than the individual $\delta^{18}O$ records themselves. Critically, this interpretive framework only holds if the three speleothem sites are isotopically connected, meaning that changes in $\delta^{18}O$ that occur at one site are propagated downwind to the other sites (Salati et al., 1979; Hu et al., 2008;

Winnick et al., 2014; Kukla et al., 2019). However, the extent to which an upwind $\delta^{18}O$ signal is transferred downwind between sites is difficult to constrain with reanalysis data. Instead, we quantify the moisture recycling connectivity, or how much moisture reaches two sites along a transect. Moisture that is recycled across both sites of a transect will necessarily carry the isotopic signature of its upwind rainout and evaporation.

To validate our use of the isotope gradient approach, we quantify the moisture recycling connectivity of the three sites using the two-atmospheric-layer water accounting model (WAM-2layers) of van der Ent, Wang-Erlandsson, Keys, and Savenije (2014) and the precipitation back-tracking scheme of Keys et al. (2012) (van der Ent & Savenije, 2013; van der Ent, 2016). We run the model for all three speleothem sites where each site is represented by a 3x3 grid of 1.5 degree cells, following Cluett, Thomas, Evans, and Keys (2021). The WAM-2layers forward and backward tracking schemes output evaporationsheds and precipitationsheds, respectively, where a site's evaporation-shed is the region where local evaporation re-precipitates and its precipitationshed is the region where its precipitation is sourced via evaporation. We can approximate the degree of moisture recycling connectivity by analyzing the precipitation- and evaporationshed threshold, or the probabilistic region encompassing some percentage of total rainfall, wherein two sites exist within the same "-shed" (Keys et al., 2012). A lower threshold indicates a stronger recycling connection. For example, at a given site, every grid cell contributes at least an infinitesimally small amount of vapor to local rainfall, so the 100% precipitationshed threshold encompasses the entire globe. Keys et al. (2012) set a threshold of 70% to encompass meaningful regional dynamics and moisture recycling connections for precipitationsheds. We find that the eastern and central sites are connected with a precipitationshed threshold of 36% (evaporationshed threshold of 63%), and the central and western sites with a precipitation-shed threshold of 48% (evaporation-shed threshold of 32%) (see main text).

This hydrologic connection is rather robust across the annual cycle, with upwind sites providing moisture to downwind sites throughout the wet season (Fig. S2 and year-round (Fig. S2.

These precipitation-shed thresholds likely underestimate the true moisture recycling connectivity. Precipitation-sheds only include moisture that has been recycled once (*i.e.* a single instance of evaporation and re-precipitation). However, it is likely that a substantial fraction of moisture between these sites (especially from central to western) is recycled more than once (Zemp et al., 2014), meaning not all of the moisture reaching each site is accounted for in our analysis. Additionally, the isotopic signal of upwind rainout (*i.e.* the decrease in $\delta^{18}O$ from a moisture-depleted airmass) will propagate downwind, even if the upwind precipitation itself does not. Thus, the isotopic connectivity is underestimated by the moisture recycling connectivity. Based on this result, we find that the eastern-to-central and central-to-western isotope gradients are sufficiently hydrologically connected to interpret their $\Delta\delta^{18}O$ trends. Because such a large fraction of western (central) rainout is sourced from the central (eastern) site, oxygen isotope signals at the upwind site are likely to propagate downwind in the climatological mean. This analysis indicates relative changes in $\Delta\delta^{18}O$ likely relate to air mass rainout among all sites, but we focus exclusively on the central-to-western gradient to *quantify* rainfall trends from $\Delta\delta^{18}O$ data because the trajectory aligns more closely with prevailing monsoon winds.

Text S2: Reactive transport model assumptions and limitations

The general assumptions and limitations of the RTM are described in section 2.4 of Kukla et al. (2019). Two of these limitations are relevant for our analysis. These are 1) the assumption of isotopes in precipitation reflecting mean annual conditions and 2) the limitation of the model to "single storm track" systems.

First, the implementation of the Budyko framework requires the assumption that fluxes of P, ET, and E_0 reflect climatological mean values. The limits to ET in the Budyko solution space do not apply on seasonal or even annual timescales where water storage cannot be assumed constant. This means that our model cannot meaningfully evaluate possible seasonal biases that may weaken the relationship between $\delta^{18}O$ and long-term mean conditions if changes in water storage are significant. However, we do not expect these biases to significantly influence our analysis for two reasons. First, these biases often affect single-site $\delta^{18}O$ records on a regional scale. If each study site is equally influenced by the same regional bias, this will not affect our $\Delta\delta^{18}O$ data. Second, the isotope gradient ($\Delta\delta^{18}O$) in the Amazon varies seasonally in the same direction as expected with changes in the seasonal water balance (shallower in the dry season, steeper in the wet season) (Fig. S4), suggesting the isotope gradient is a robust tracer of the mean annual water balance (as it tracks the water balance year-round).

A second limitation to the application of our model is based on the assumption of a single storm track. The RTM cannot simulate mixing between different storm trajectories and instead assumes that precipitation is delivered across a 1-dimensional domain from a single source. Presently, a robust definition for a "single storm track" remains elusive, but we note a few conditions that lend confidence to the RTM application (following Kukla et al. (2019)). First, dramatic seasonal or climatological variability in the direction of moisture transport is incompatible with the RTM. Despite the monsoon climate of

the Amazon Basin, seasonal changes in wind direction do not appear to strongly bias the $\Delta\delta^{18}O$, as evidenced in the application to modern data in Kukla et al. (2019) and the good agreement between simulated mean annual precipitation in our Pre-Industrial (LH) Monte Carlo simulations. This could be due to similar transport distances across the continent between seasons (despite its "monsoon" designation, wind directions in South America show less seasonal variability than most other monsoonal regions), possible incorporation of wet season rain in dry season moisture, or that even seasonal changes in monsoonal wind directions are not great enough to violate the single storm track assumption.

Text S3: Isotopic effects of convection

A number of previous studies have demonstrated that both micro- and macro-physical processes associated with deep convection may result in a number of distinct isotopic effects on resulting precipitation. Microphysical processes are unlikely to be the main driver of the "amount effect" as it is well-documented that the correlation between $\delta^{18}O$ and precipitation amount breaks down at small scales (Kurita et al., 2009; Moerman et al., 2013; Moore et al., 2014; Aggarwal et al., 2016; Conroy et al., 2016; Konecky et al., 2019). In its original formulation, the RTM used here does not explicitly simulate convective processes like vertical downdrafts and dry air entrainment, altitude-dependent changes in vertical velocity, and precipitation efficiency. In this section, we describe the possible isotopic effects associated with convective processes, the baseline representation of macro-scale processes such precipitation efficiency, re-evaporation, and stratiform versus convective rain in our model framework, and a model sensitivity analysis to post-condensation evaporation.

Recycling of water vapor in the convective cloud and stratiform vs. convective rain

Previous studies have shown that two primary sources contribute to moisture within convective clouds 1) an oceanic source and 2) a local, sub-cloud evaporation source. These two sources are explicitly represented in our mass balance equations, as the moisture available for precipitation is the sum of transported and local surface-evapotranspired vapor. Indeed, the balance between these two sources is widely cited as the primary driver of the tropical "amount effect"—the negative correlation between $\delta^{18}O$ and precipitation amount (Rozanski et al., 1993; Lee & Fung, 2008; Lee et al., 2009; Moore et al., 2014; Bailey et al., 2018). Because transport balances precipitation minus evapotranspiration, the ratio of transported to evapotranspired moisture (γ) can be represented by:

$$\gamma \equiv -\frac{P-E}{E} \tag{1}$$

Where P is precipitation and E is evaporation. The "amount effect" emerges because in tropical oceans and most tropical land masses (including Amazonia), E is limited by potential evapotranspiration or the energy available for evaporation, such that P is the primary driver of changes in γ (potential evaporation does not vary much in the tropics). Thus the constraint of potential evapotranspiration on evapotranspiration provides a robust representation of the "amount effect" as the balance of P and E in our model.

We note that an alternative hypothesis for the tropical "amount effect" argues that it is driven by the proportion of convective versus stratiform precipitation (Kurita, 2013; Aggarwal et al., 2016; Konecky et al., 2019). However, large scale circulation that generates stratiform precipitation balances P-minus-E (numerator of equation 1), whereas convection mostly sources local evaporation (denominator of equation 1) (Moore et al., 2014). Thus, the balance of convective and stratiform precipitation is necessarily related to γ (Moore et al., 2014) which is represented in our model.

Sensitivity analysis of post-condensation re-evaporation

In atmospheric circulation models, re-evaporation determines how much condensed vapor reaches the ground as precipitation (i.e. "precipitation efficiency"). Precipitation efficiency parameterizations exert significant influence over modeled climate and are often used as tuning parameters for global hydroclimate as in the MERRA2 reanalysis product (Bacmeister et al., 2006; Molod et al., 2015).

However, the extent of isotopic effects of post-condensation evaporation is not well characterized. Theoretically, the extent of fractionation during re-evaporation depends primarily on whether all raindrops partially re-evaporate to a similar extent (large frac-

tionation signal) or if re-evaporation is skewed towards the full evaporation of smaller droplets with minimal partial evaporation of larger droplets (minimal fractionation signal). Drop sizes and their role in re-evaporation are usually parameterized and are not well-constrained (e.g. Lee and Fung (2008)). Thus, while MERRA2 reanalysis estimates 50-60% of tropical condensed moisture evaporates before reaching land (Konecky et al., 2019) the magnitude of isotopic effects are not well characterized.

Observational studies have aimed to quantify the effect of re-evaporation on vapor and precipitation isotopes (Worden et al., 2007; Konecky et al., 2019). Direct measurements of this effect are extremely difficult, and existing studies rely on correlations between isotopes and climate conditions. For example, Worden et al. (2007) use Tropospheric Emission Spectrometer (TES) data to argue low δD at high specific humidity in the tropics is due to re-evaporation. However, whether the TES can resolve re-evaporation signals in convection remains an open question (Duan et al., 2018). Using direct precipitation measurements, Konecky et al. (2019) notes a correlation between $\delta^{18}O$ of precipitation and MERRA2 estimates of rainfall re-evaporation, though confounding factors such as the stratiform fraction (or P/E balance) may influence this relationship as they are used to calculate re-evaporation in MERRA2 (Bacmeister et al., 2006; Molod et al., 2015). Thus, while observational studies indicate correlations between local rainfall $\delta^{18}O$ and metrics of re-evaporation, it remains unclear how sensitive $\delta^{18}O$ is to re-evaporation alone. Additionally, cloud-resolving model simulations suggest that re-evaporation has a minimal effect on the isotopic "amount effect" (Moore et al., 2014).

Isotope-enabled models calibrated to global precipitation $\delta^{18}O$ also indicate minimal isotopic effects of post-condensation evaporation. Dee, Noone, Buenning, Emile-Geay, and Zhou (2015) calibrate re-evaporation to global $\delta^{18}O$ data using an isotope-enabled, simple-physics atmospheric GCM, "SPEEDY-IER". Their approach may help disentan-

gle how much of the total re-evaporation flux affects isotopes (via partial drop evaporation). They find that the spatial distribution of isotopes is strongly influenced by the re-evaporation parameterization. Using the re-evaporation formulation of Sundqvist (1988), re-evaporation (Eprec) in SPEEDY-IER is:

$$E_{prec} = K_E(1-h)\sqrt{P} \tag{2}$$

Where E_{prec} depends on humidity (h), precipitation (P) and a coefficient K_E. E_{prec} increases with lower humidity and with more precipitation. However, isotope fractionation is proportional to the fraction of evaporated moisture (E_{prec}/P) and the re-evaporation fraction decreases as precipitation (P) increases. Dee et al. (2015) find that K_E of $\sim$0.03 provides the best fit to global $\delta^{18}O$ (where fluxes have units of g m-2 s-1). With this parameterization, the re-evaporation fraction is far lower than MERRA2 suggests for the tropics, suggesting that most re-evaporation involves total droplet evaporation and does not affect precipitation $\delta^{18}O$.

To test the sensitivity of our results to post-condensation re-evaporation effects, we modify the isotope module of our RTM to include the re-evaporation fraction and force it with three scenarios following the parameterization of Dee et al. (2015) (Fig. S6). The first is a control scenario where we initialize the RTM with Amazon climatology and no re-evaporation flux. In the second scenario we assume the unlikely case that re-evaporation affects the $\delta^{18}O$ of all raindrops equally, regardless of size. We assume tropical E_{prec}/P is 0.55 (from the range of Konecky et al. (2019)). This is the largest effect re-evaporation could have on $\delta^{18}O$ but is unlikely because it does not account for total re-evaporation of the smallest droplets (Lee & Fung, 2008) and is inconsistent with isotope-enabled climate model calibrations. In the third scenario we assume the isotopic effect of re-evaporation

follows the parameterization of (Dee et al., 2015). Adopting the conservative (highest E_{prec}/P) estimates of P=2.4m/yr and h=0.5 we find E_{prec}=0.05 in the Amazon (equation 1). Higher values of h and P, both expected on the timescale of a storm event when E_{prec} matters for precipitation, lead to lower E_{prec}/P and therefore an even smaller effect on precipitation $\delta^{18}O$.

We use the RTM to interpret the spatial isotope gradient rather than absolute $\delta^{18}O$ values (Fig. S6), so we discuss the effect of re-evaporation on RTM $\Delta\delta^{18}O$ here. When all re-evaporation leads to isotope fractionation, the modeled isotope gradient is -2.8‰/1,000km, steeper than the steepest isotope gradient documented in the last ∼40 kyr (the extent of the proxy data; -2.5‰/1,000km). By contrast, when the RTM is run with E_{prec}/P values derived from the optimization of Dee et al. (2015), re-evaporation has a negligible effect on $\Delta\delta^{18}O$, leading to a decrease of only 0.08‰/1,000km which is well within the uncertainty from the proxy data (+/- 0.3‰/1,000 km) (Fig. S6).

Taken together, we maintain that it is appropriate to omit a re-evaporation scheme in our analysis in the main text for three reasons: 1) There is no strong observational evidence supporting a large-scale link between isotopes and re-evaporation; 2) the RTM is successful at simulating modern precipitation $\delta^{18}O$ when forced with modern climatology, suggesting it already represents the important physical processes; and 3) The globally-calibrated parameterization of Dee et al. (2015) suggests tropical precipitation $\delta^{18}O$ is insensitive to the incorporation of re-evaporation into our model. The Dee et al. (2015) parameterization optimizes the fit to modern precipitation $\delta^{18}O$ and, therefore, serves as an indication of how re-evaporation affects the isotope balance. The discrepancy between the large re-evaporation rates required to simulate tropical hydroclimate (e.g. (Bacmeister et al., 2006; Molod et al., 2015; Konecky et al., 2019)) and the small re-evaporation rates required to simulate its isotopes (Dee et al., 2015); Fig. S6) suggests that re-

evaporation mostly occurs by the total evaporation of smaller raindrops that have no effect on precipitation $\delta^{18}O$.

Text S4: Comparing the three speleothem $\delta^{18}O$ signals to global records

To contextualize our estimated change in Amazon rainfall from the LGM to the mid-Holocene and begin hypothesizing the underlying dynamic driver, we compare the magnitude of $\delta^{18}O$ change at each site (eastern, central, and western) to similar global records. We compile all records from the SISALv2 database that span more than 10000 years (Atsawawaranunt et al., 2018; Comas-Bru et al., 2019, 2020), the approximate duration from the peak-to-trough of a precession cycle. We filter out records that are exceptionally long ($>$ 100kyr) because the range of $\delta^{18}O$ increases with the duration of the record above this threshold, but is mostly independent of the record duration below. Finally, we only analyze records with an absolute latitude less than 40 degrees to isolate tropical and subtropical climates. To account for variations from site to site in the high-frequency "noise" of the data, all records are smoothed with a 1000 yr moving average and re-sampled to the same resolution (including the tropical South America sites). We calculate the standard deviation (not shown) and range of each record and compare to the three records of interest.

Text S5: Toy model of phase of precipitation seasonality and $\Delta\delta^{18}O$

The goal of this section is to test whether the phase of precipitation seasonality can impact $\Delta\delta^{18}O$ independent of net rainout. We simulate $\Delta\delta^{18}O$ between two sites throughout the year, varying the difference in the phase of precipitation seasonality and the amplitude of seasonal $\delta^{18}O$ (thus, $\Delta\delta^{18}O$). We first prescribe some seasonal cycle of precipitation upwind of site 1 (the eastern, or upwind site). Since we only care about differences in the phase of precipitation seasonality between sites (and, being the tropics, we ignore temperature seasonality), we hold the upwind seasonal cycle of precipitation constant. Upwind rainout at site 1 set as:

$$P_{s1,upwind} = A \times cos\left(2\pi \times t\right) + A \tag{3}$$

where A is the amplitude, t is time (fraction of year from zero to one), and the amplitude is added to the end to avoid negative precipitation rates. $P_{s1,upwind}$ represents the integrated upwind rainout that occurs at the upwind site. We then calculate $P_{s2,upwind}$, the integrated rainout between sites (upwind of site 1, downwind of site 2), using the same sine curve as $P_{s1,upwind}$ with some phase shift, ϕ:

$$P_{s2,upwind} = A \times cos\left(2\pi \times t + \phi\right) + A. \tag{4}$$

The oxygen isotope composition of rainfall at the upwind site (site 1) is calculated assuming that source moisture $\delta^{18}O$ equals zero and $\delta^{18}O$ is anti-correlated with upwind rainfall with some slope, m:

$$\delta^{18}O_{s1} = 0 - \left(\frac{P_{s1,upwind}}{m}\right). \tag{5}$$

Downwind $\delta^{18}O$ (site 2) is calculated the same way, just substituting $\delta^{18}O_{s1}$ for zero:

$$\delta^{18}O_{s2} = \delta^{18}O_{s1} - \left(\frac{P_{s2,upwind}}{m}\right). \tag{6}$$

Finally, we take the $\delta^{18}O$ difference between sites to get $\Delta\delta^{18}O$, then calculate the climatological $\Delta\delta^{18}O$ by taking the precipitation-weighted annual mean. We repeat these calculations for changes in the phase, ϕ, and relative $\delta^{18}O$ seasonal amplitude, captured by the slope term m. The results are shown in Figs. S11 and S12.

The model results show that changes in the relative phase of precipitation from one site to the next do not invalidate $\Delta\delta^{18}O$ as a proxy for net rainout. The error introduced by phase differences between sites is non-zero, but it is negligible—consistently less than 1% of the seasonal amplitude of $\Delta\delta^{18}O$. Given a $\Delta\delta^{18}O$ seasonal amplitude of $\sim$2‰/1000km from the eastern-to-central sites today, differences in the timing of eastern and central peak precipitation should impact $\Delta\delta^{18}O$ by less than 0.02‰/1000 km.

Text S6: Testing seasonal climate anomalies with results of Liu & Battisti, 2015

Liu & Battisti show that, in their simulations, the decrease in $\delta^{18}O$ in northeastern Brazil as austral summer insolation decreases is driven by more DJFMA precipitation and lower wet-season $\delta^{18}O$. Here, we analyze how their seasonal precipitation and $\delta^{18}O$ anomalies can be reconciled with the observed amplitude of northeastern Brazil $\delta^{18}O$ change of ∼5-7‰. We digitize their monthly northeastern Brazil results (Fig. 7 of Liu and Battisti (2015)) using Engauge Digitizer (Fig. S8A), and we test three sets of simulated anomalies (Fig. S8B). First, we test whether increasing wet season (DJFMA) and decreasing dry season (JJA) rainfall can cause a 5-7‰ $\delta^{18}O$ shift, holding the seasonal cycle of $\delta^{18}O$ constant. Because JJA rainfall is at zero for their high- and low-insol experiments, we use the modern observed precipitation seasonality for the control case. We find no reasonable change in precipitation seasonality that is capable of explaining the amplitude of eastern $\delta^{18}O$ change.

Next, we test the role of JJA and DJFMA precipitation $\delta^{18}O$ anomalies. Due to low JJA rainfall (even using modern observations as the initial, control case) JJA $\delta^{18}O$ has a negligible effect on precipitation-weighted $\delta^{18}O$, whereas DJFMA $\delta^{18}O$ has a much larger effect. Still, DJFMA $\delta^{18}O$ would have to decrease by 5-7‰ relative to the high_insol case in order to match the eastern domain $\delta^{18}O$ record (about a 4x larger change in $\delta^{18}O$ than found in the simulations of Liu and Battisti (2015). This result holds even in our third experiment, where we allow DJFMA precipitation amounts to increase. We conclude that, given the simulated seasonal cycle of precipitation or $\delta^{18}O$ in Liu and Battisti (2015), a much larger decrease in wet-season $\delta^{18}O$ is required to explain the eastern speleothem $\delta^{18}O$ data—consistent with a zonal shift in the precipitation centroid.

Figures S1-S12

References

Aggarwal, P. K., Romatschke, U., Araguas-Araguas, L., Belachew, D., Longstaffe, F. J., Berg, P., ... Funk, A. (2016, August). Proportions of convective and stratiform precipitation revealed in water isotope ratios. *Nature Geoscience*, *9*(8), 624–629. doi: 10.1038/ngeo2739

Atsawawaranunt, K., Comas-Bru, L., Mozhdehi, S. A., Deininger, M., Harrison, S. P., Baker, A., ... Scroxton, N. (2018). The SISAL database: A global resource to document oxygen and carbon isotope records from speleothems. *Earth System Science Data*, *10*, 1687–1713.

Bacmeister, J. T., Suarez, M. J., & Robertson, F. R. (2006, December). Rain Reevaporation, Boundary Layer–Convection Interactions, and Pacific Rainfall Patterns in an AGCM. *Journal of the Atmospheric Sciences*, *63*(12), 3383–3403. doi: 10.1175/JAS3791.1

Bailey, A., Posmentier, E., & Feng, X. (2018, July). Patterns of evaporation and precipitation drive global isotopic changes in atmospheric moisture. *Geophysical Research Letters*, *45*, 7093–7101. doi: 10.1029/2018GL078254

Chamberlain, C. P., Winnick, M. J., Mix, H. T., Chamberlain, S. D., & Maher, K. (2014). The impact of neogene grassland expansion and aridification on the isotopic composition of continental precipitation. *Global Biogeochemical Cycles*, *28*(9), 992–1004. doi: 10.1002/2014GB004822

Cluett, A. A., Thomas, E. K., Evans, S. M., & Keys, P. W. (2021, June). Seasonal Variations in Moisture Origin Explain Spatial Contrast in Precipitation Isotope Seasonality on Coastal Western Greenland. *Journal of Geophysical Research: Atmospheres*,

126(11). doi: 10.1029/2020JD033543

Comas-Bru, L., Harrison, S. P., Werner, M., Rehfeld, K., Scroxton, N., Veiga-Pires, C., & SISAL working group members. (2019, August). Evaluating model outputs using integrated global speleothem records of climate change since the last glacial. *Climate of the Past*, *15*(4), 1557–1579. doi: 10.5194/cp-15-1557-2019

Comas-Bru, L., Rehfeld, K., Roesch, C., Amirnezhad-Mozhdehi, S., Harrison, S. P., Atsawawaranunt, K., ... SISAL Working Group members (2020, October). SISALv2: A comprehensive speleothem isotope database with multiple age–depth models. *Earth System Science Data*, *12*(4), 2579–2606. doi: 10.5194/essd-12-2579-2020

Conroy, J. L., Noone, D., Cobb, K. M., Moerman, J. W., & Konecky, B. L. (2016, April). Paired stable isotopologues in precipitation and vapor: A case study of the amount effect within western tropical Pacific storms: Isotopes in Western Pacific Storms. *Journal of Geophysical Research: Atmospheres*, *121*(7), 3290–3303. doi: 10.1002/2015JD023844

Dee, S., Noone, D., Buenning, N., Emile-Geay, J., & Zhou, Y. (2015, January). SPEEDY-IER: A fast atmospheric GCM with water isotope physics. *Journal of Geophysical Research: Atmospheres*, *120*(1), 73–91. doi: 10.1002/2014JD022194

Duan, S. Q., Wright, J. S., & Romps, D. M. (2018, February). On the Utility (or Futility) of Using Stable Water Isotopes to Constrain the Bulk Properties of Tropical Convection. *Journal of Advances in Modeling Earth Systems*, *10*(2), 516–529. doi: 10.1002/2017MS001074

Hu, C., Henderson, G. M., Huang, J., Xie, S., Sun, Y., & Johnson, K. R. (2008, February). Quantification of Holocene Asian monsoon rainfall from spatially separated cave records. *Earth and Planetary Science Letters*, *266*(3-4), 221–232. doi: 10.1016/j.epsl.2007.10.015

Keys, P. W., van der Ent, R. J., Gordon, L. J., Hoff, H., Nikoli, R., & Savenije, H. H. G. (2012, February). Analyzing precipitationsheds to understand the vulnerability of rainfall dependent regions. *Biogeosciences*, *9*(2), 733–746. doi: 10.5194/bg-9-733-2012

Konecky, B. L., Noone, D. C., & Cobb, K. M. (2019, February). The Influence of Competing Hydroclimate Processes on Stable Isotope Ratios in Tropical Rainfall. *Geophysical Research Letters*, *46*(3), 1622–1633. doi: 10.1029/2018GL080188

Kukla, T., Winnick, M. J., Maher, K., Ibarra, D. E., & Chamberlain, C. P. (2019, January). The Sensitivity of Terrestrial δ ^{18} O Gradients to Hydroclimate Evolution. *Journal of Geophysical Research: Atmospheres*, *124*, 563–582. doi: 10.1029/2018JD029571

Kurita, N. (2013, September). Water isotopic variability in response to mesoscale convective system over the tropical ocean: ISOTOPES IN OCEANIC MOISTURE. *Journal of Geophysical Research: Atmospheres*, *118*(18), 10,376–10,390. doi: 10.1002/jgrd.50754

Kurita, N., Ichiyanagi, K., Matsumoto, J., Yamanaka, M. D., & Ohata, T. (2009, September). The relationship between the isotopic content of precipitation and the precipitation amount in tropical regions. *Journal of Geochemical Exploration*, *102*(3), 113–122. doi: 10.1016/j.gexplo.2009.03.002

Lee, J.-E., & Fung, I. (2008). "Amount effect" of water isotopes and quantitative analysis of post-condensation processes. *Hydrological Processes*, *2274*(November 2008), 2267–2274. doi: 10.1002/hyp

Lee, J.-E., Johnson, K., & Fung, I. (2009). Precipitation over South America during the Last Glacial Maximum: An analysis of the "amount effect" with a water isotope-enabled general circulation model. *Geophysical Research Letters*, *36*(19), L19701.

doi: 10.1029/2009GL039265

Liu, X., & Battisti, D. S. (2015, June). The Influence of Orbital Forcing of Tropical Insolation on the Climate and Isotopic Composition of Precipitation in South America. *Journal of Climate*, *28*(12), 4841–4862. doi: 10.1175/JCLI-D-14-00639.1

Moerman, J. W., Cobb, K. M., Adkins, J. F., Sodemann, H., Clark, B., & Tuen, A. A. (2013, May). Diurnal to interannual rainfall δ18O variations in northern Borneo driven by regional hydrology. *Earth and Planetary Science Letters*, *369–370*, 108–119. doi: 10.1016/j.epsl.2013.03.014

Molod, A., Takacs, L., Suarez, M., & Bacmeister, J. (2015, May). Development of the GEOS-5 atmospheric general circulation model: Evolution from MERRA to MERRA2. *Geoscientific Model Development*, *8*(5), 1339–1356. doi: 10.5194/gmd-8-1339-2015

Moore, M., Kuang, Z., & Blossey, P. N. (2014). A moisture budget perspective of the amount effect. *Geophysical Research Letters*, *41*(4), 1329–1335. doi: 10.1002/2013GL058302

Rozanski, K., Araguás-Araguás, L., & Gonfiantini, R. (1993). Isotopic Patterns in Modern Global Precipitation. *Climate Change in Continental Isotopic Records*, *78*, 1–36. doi: 10.1029/GM078p0001

Salati, E., Dall'Olio, A., Matsui, E., & Gat, J. R. (1979). Recycling of water in the Amazon Basin: An isotopic study. *Water Resources Research*, *15*(5), 1250–1258. doi: 10.1029/WR015i005p01250

Sundqvist, H. (1988). Parameterization of Condensation and Associated Clouds in Models for Weather Prediction and General Circulation Simulation. In M. E. Schlesinger (Ed.), *Physically-Based Modelling and Simulation of Climate and Climatic Change* (pp. 433–461). Dordrecht: Springer Netherlands. doi: 10.1007/978-94-009-3041-4_10

van der Ent, R. J. (2016). *WAM-2layers Python.*

van der Ent, R. J., & Savenije, H. H. G. (2013, July). Oceanic sources of continental precipitation and the correlation with sea surface temperature: Precipitation and Correlation with SST. *Water Resources Research*, *49*(7), 3993–4004. doi: 10.1002/wrcr.20296

van der Ent, R. J., Wang-Erlandsson, L., Keys, P. W., & Savenije, H. H. G. (2014, December). Contrasting roles of interception and transpiration in the hydrological cycle – Part 2: Moisture recycling. *Earth System Dynamics*, *5*(2), 471–489. doi: 10.5194/esd-5-471-2014

Winnick, M. J., Chamberlain, C. P., Caves, J. K., & Welker, J. M. (2014). Quantifying the isotopic 'continental effect'. *Earth and Planetary Science Letters*, *406*, 123–133. doi: 10.1016/j.epsl.2014.09.005

Worden, Noone, D., Bowman, K., & Tropospheric Emission Spectrometer science team and data. (2007, February). Importance of rain evaporation and continental convection in the tropical water cycle. *Nature*, *445*(7127), 528–532. doi: 10.1038/nature05508

Zemp, D. C., Schleussner, C.-F., Barbosa, H. M. J., van der Ent, R. J., Donges, J. F., Heinke, J., ... Rammig, A. (2014, December). On the importance of cascading moisture recycling in South America. *Atmospheric Chemistry and Physics*, *14*(23), 13337–13359. doi: 10.5194/acp-14-13337-2014

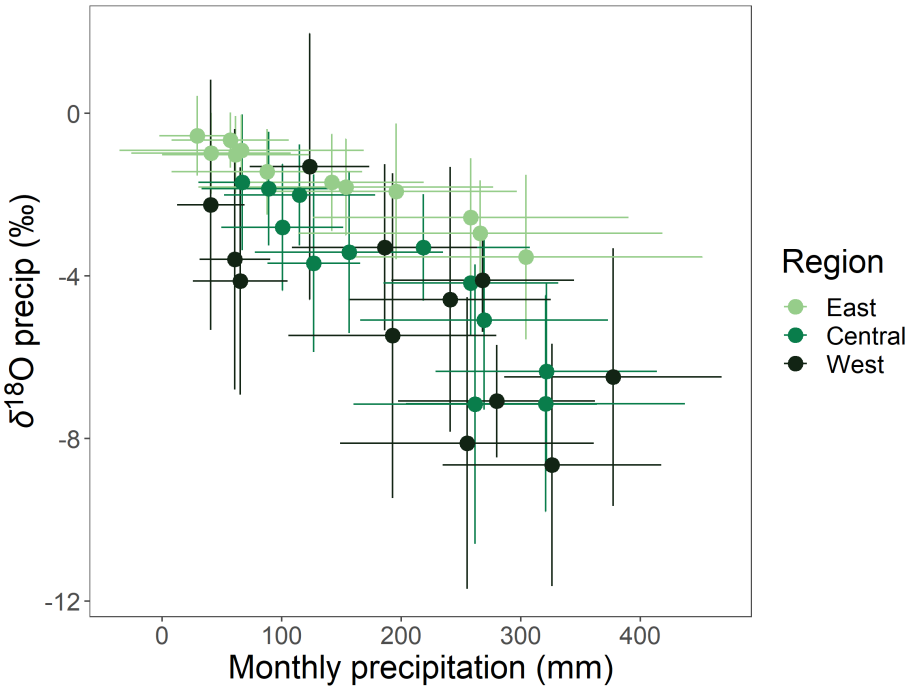

Figure S1. Relationship between $\delta^{18}O$ of modern precipitation and precipitation amount for eastern, central, and western tropical South America. All points are monthly means from GNIP. Slope of east region is similar or shallower than central and west, indicating same or larger precipitation change for the same $\delta^{18}O$. Eastern sites: Fortaleza, Ceara Mirim, Cachimbo; Central sites: Manaus, Manaus Piracicaba, Santarem; Western sites: Cruzeiro do Sul, Benjamin Constant, Porto Velho, Rio Branco.

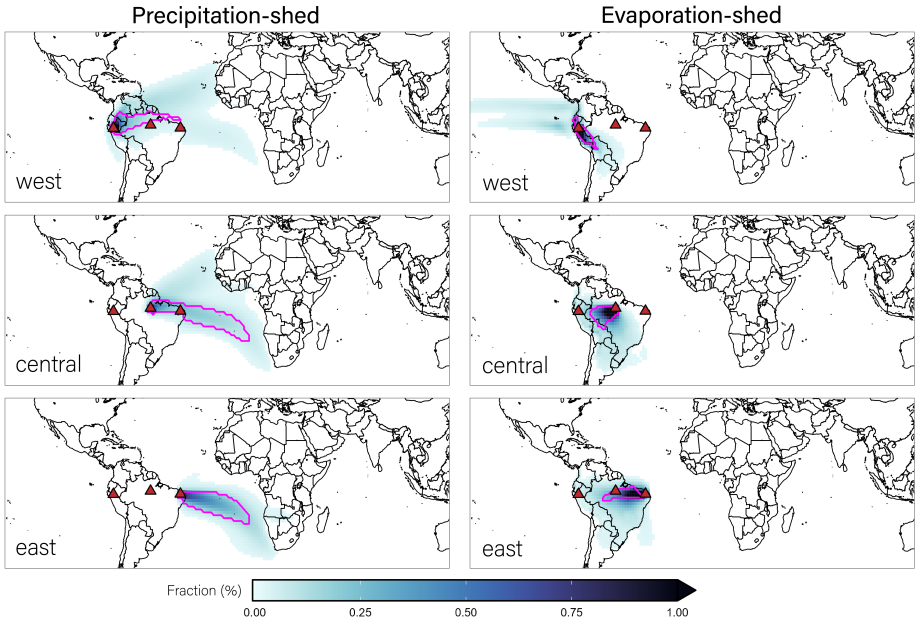

Figure S2. NDJFMAM (wet season) Two-layer WAM results using climatological mean of ERA interim reanalysis. Magenta contour line is the 70% threshold, used to indicate a dynamic connection. Note that WAM-2layers computes one round of moisture recycling, whereas some moisture likely requires more than one precipitation-evaporation cycle to reach from west to east. Generally, evaporation from upwind (east) sites is within the precipitation-shed of downwind (west) sites.

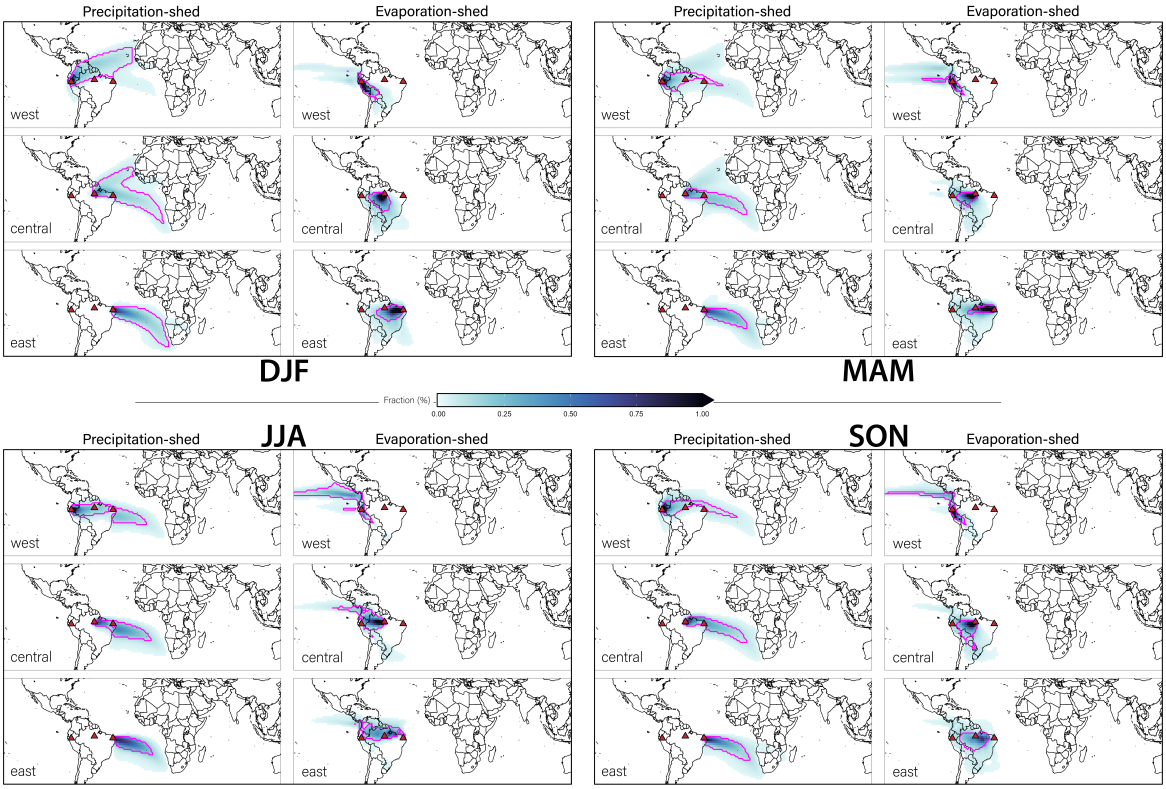

Figure S3. Seasonal Two-layer WAM results using climatological mean of ERA interim reanalysis. Same as above, but separated by season. DJF is December, January, February; MAM is March, April, May; JJA is June, July, August; and SON is September, October, November.

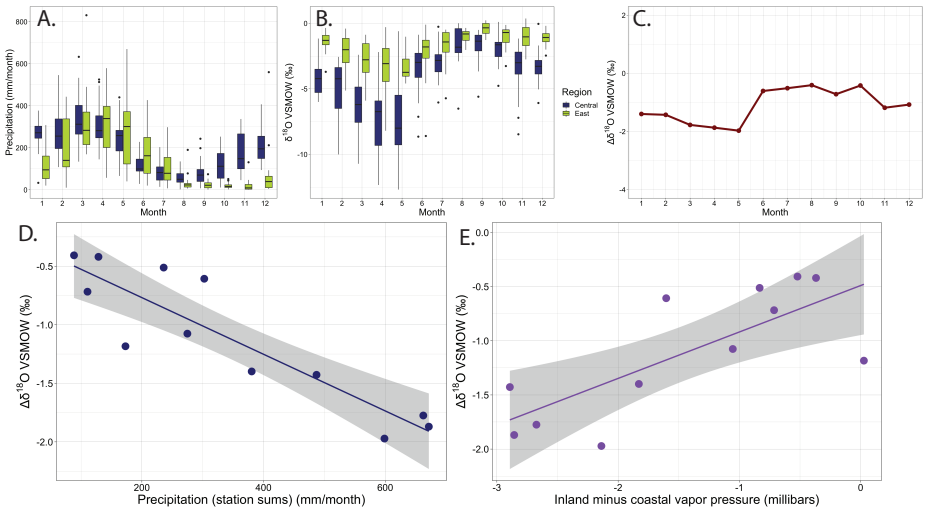

Figure S4. (**A**) Monthly precipitation rates for the Manaus GNIP station (closest to central $\delta^{18}O$ record; purple) and the Fortaleza station (closest to eastern $\delta^{18}O$ record; green). (**B**) Same as A but the isotopic composition of rainfall. (**C**) The isotope gradient between the two stations throughout the year. (**D**) Negative correlation between the isotope gradient and the sum of station precipitation indicates "amount effect"-type relationships hold across the domain on a seasonal basis. (**E**) Positive correlation between the isotope gradient and the vapor pressure difference indicates that a greater change in $\delta^{18}O$ tracks a greater change in the vapor pressure (vapor pressure values are corrected to account for an annually higher background vapor pressure in the more humid central site). All data from GNIP.

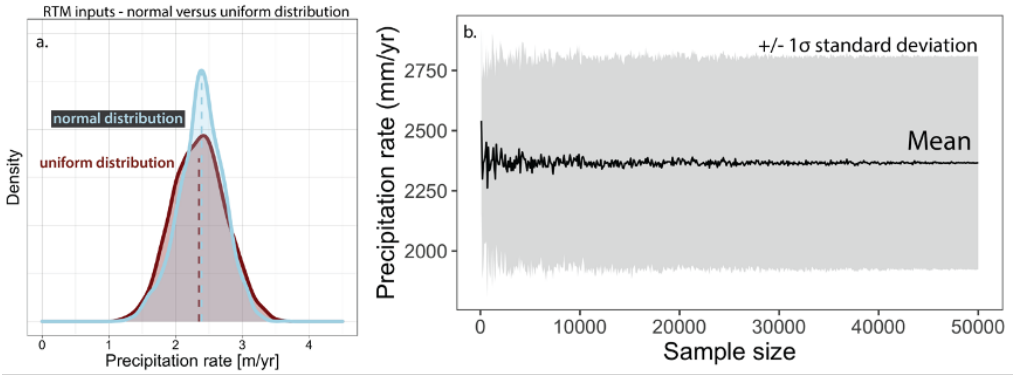

Figure S5. RTM input sensitivity and Monte Carlo diagnostics. (**A**) Comparison between assigning a uniform (dark red) versus normal (light blue) distribution to the RTM input parameters. Normal distribution leads to a narrower range of precipitation estimates. We adopt the uniform distribution for our analysis so the uncertainty on our estimates is conservative. (**B**) The mean and standard deviation of the precipitation rate stabilizes quickly, indicating the full model solution space is explored within ∼30,000 iterations.

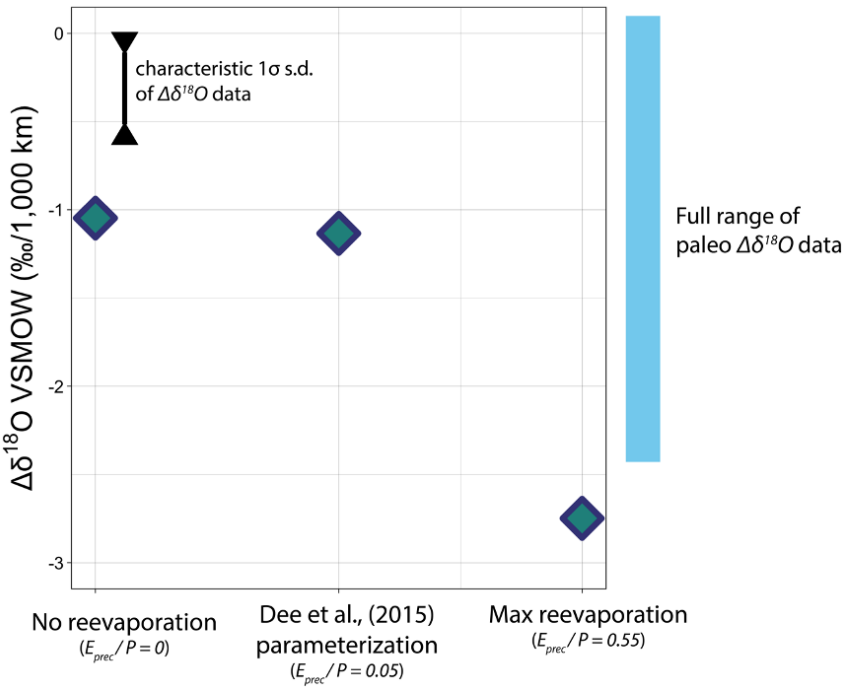

Figure S6. Effect of re-evaporation on RTM $\Delta\delta^{18}O$. Fractionation increases with E_{prec}/P (where E_{prec} is the evaporation flux of partially evaporated of raindrops, or raindrops whose evaporation influences $\delta^{18}O$). The isotope-based parameterization of re-evaporation in Dee et al. (2015) gives low E_{prec}/P in tropical conditions, suggesting most tropical re-evaporation (55% of P from MERRA2) has no effect on the isotopes of precipitation.

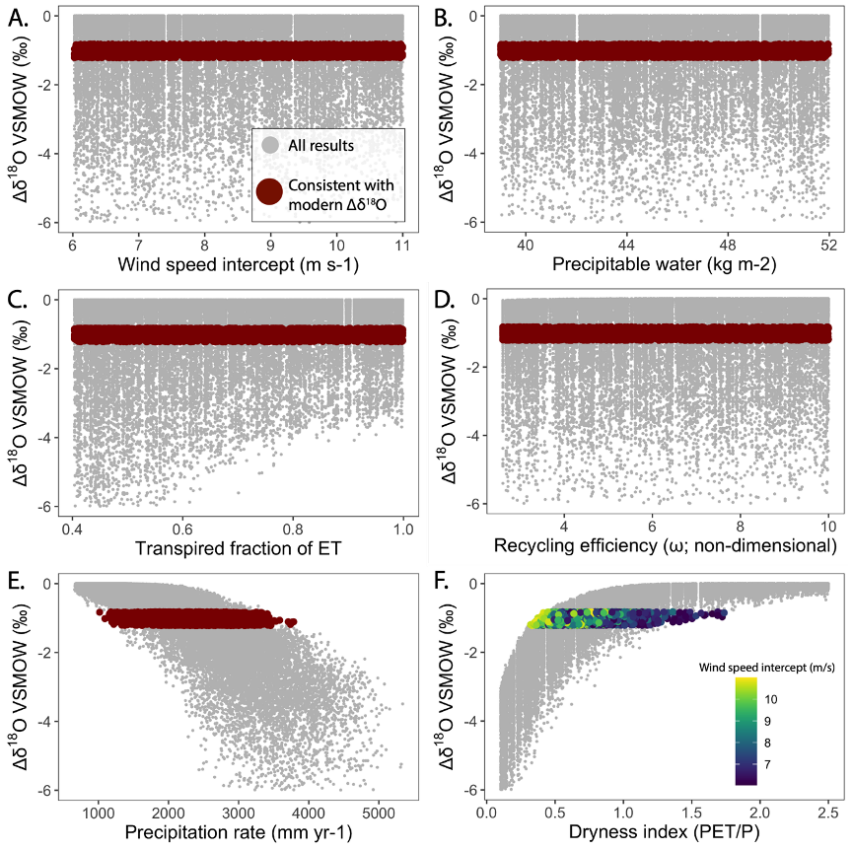

Figure S7. Monte Carlo output diagnostics for modern simulations. While all variables influence $\Delta\delta^{18}O$, opposing shifts in other terms cancel out the effect such that there is no unique solution for most variables (**A-D**). This is not the case, however, for the fluxes controlling the water balance. Both precipitation and, by consequence, the dryness index (defined as the ratio of potential ET to precipitation) have a finite set of solutions for a given $\Delta\delta^{18}O$ (**E, F**). The uncertainty in the other variables is important for building a broad, conservative uncertainty envelope in our precipitation reconstruction. For example, if we sampled a smaller range of wind speed intercepts our solution would be restricted to a smaller range of dryness indices (**F**).

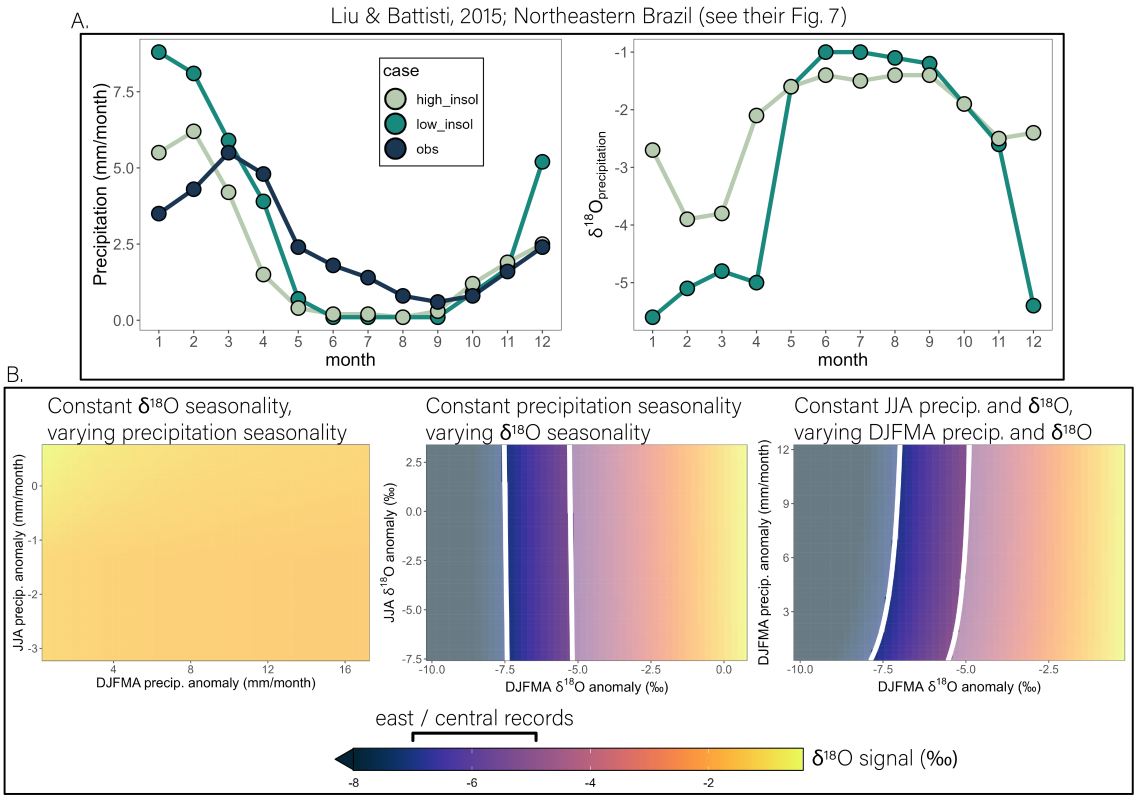

Figure S8. Changes in precipitation and $\delta^{18}O$ required to reach 5-7‰ signal with Liu & Battisti, 2015 results. (**A**) Northeastern Brazil monthly precipitation and $\delta^{18}O$ under low austral summer insolation (teal), high austral summer insolation (lightest blue), and modern observations (dark blue). Data from Fig. 7 of Liu and Battisti (2015), digitized using EngaugeDigitizer. (**B**) Effect of modifying precipitation anomaly (left), $\delta^{18}O$ anomaly (middle), or summer (DJFMA) precipitation *and* $\delta^{18}O$ anomalies (right) on the amplitude of the $\delta^{18}O$ signal. White lines denote region consistent with observations (color is grayed out outside the lines). Matching observations requires ∼4x larger DJFMA $\delta^{18}O$ shift than found in simulations of Liu and Battisti (2015). The $\delta^{18}O$ signal is not very sensitive to the JJA precipitation anomaly, the JJA $\delta^{18}O$ anomaly, nor the DJF precipitation anomaly.

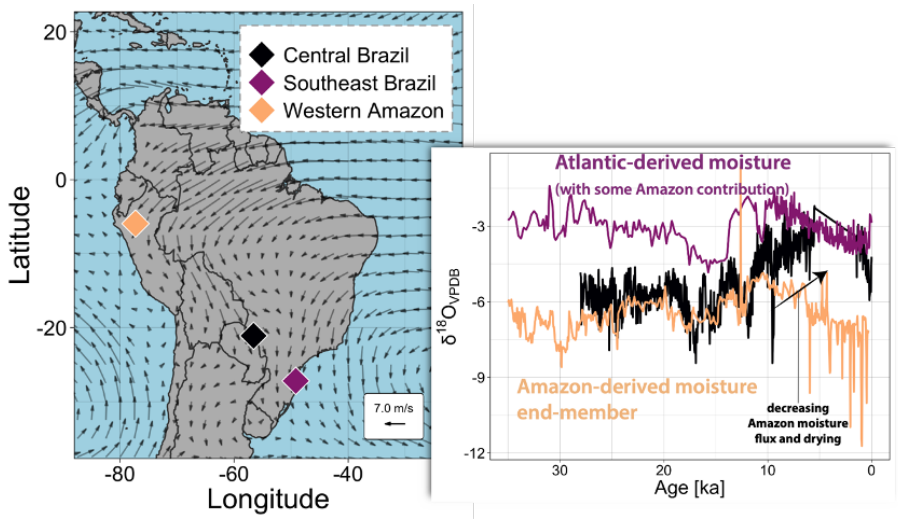

Figure S9. Amazon vs Atlantic moisture trajectories. (**Left**) Map of three speleothem sites shown in the isotope data to the right. (**Right**) Isotope records of three sites. Moisture is transported out of Amazonia from the northwesternmost site (tan diamond and line) via the Andean Low Level Jet (LLJ) to the southeasternmost site (purple diamond and line). LLJ moisture mixes with higher-$\delta^{18}O$, Atlantic-derived moisture with the maximum Atlantic contribution occurring on the coast (purple diamond). The intermediate site (black diamond and line) reflects the balance of the Amazon-derived endmember and the Atlantic endmember. $\delta^{18}O$ in the central site (black line) is similar to the Amazon-derived $\delta^{18}O$ (tan) from ~28-12 ka, indicating most precipitation comes from the LLJ. After 12 ka, $\delta^{18}O$ at the central site increases toward the southeastern (purple) values, reflecting a decrease in the LLJ moisture flux contribution as the region undergoes drying.

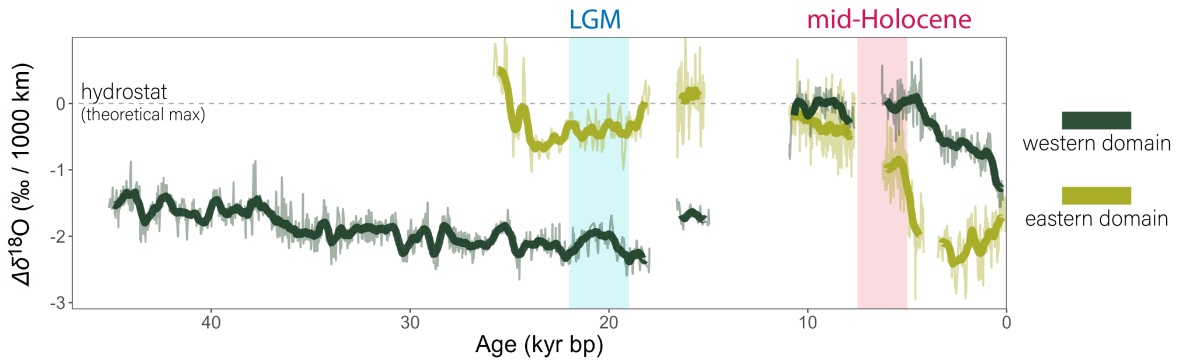

Figure S10. Extended isotope gradient proxy record. As in main text, but with extended western record to show lack of precession signal. More negative $\Delta\delta^{18}O$ reflects more rainout and wetter conditions. $\Delta\delta^{18}O$ of zero is the theoretical maximum value (the "hydrostat"; (Chamberlain et al., 2014; Kukla et al., 2019)) and reflects the approximate balance of P and ET.

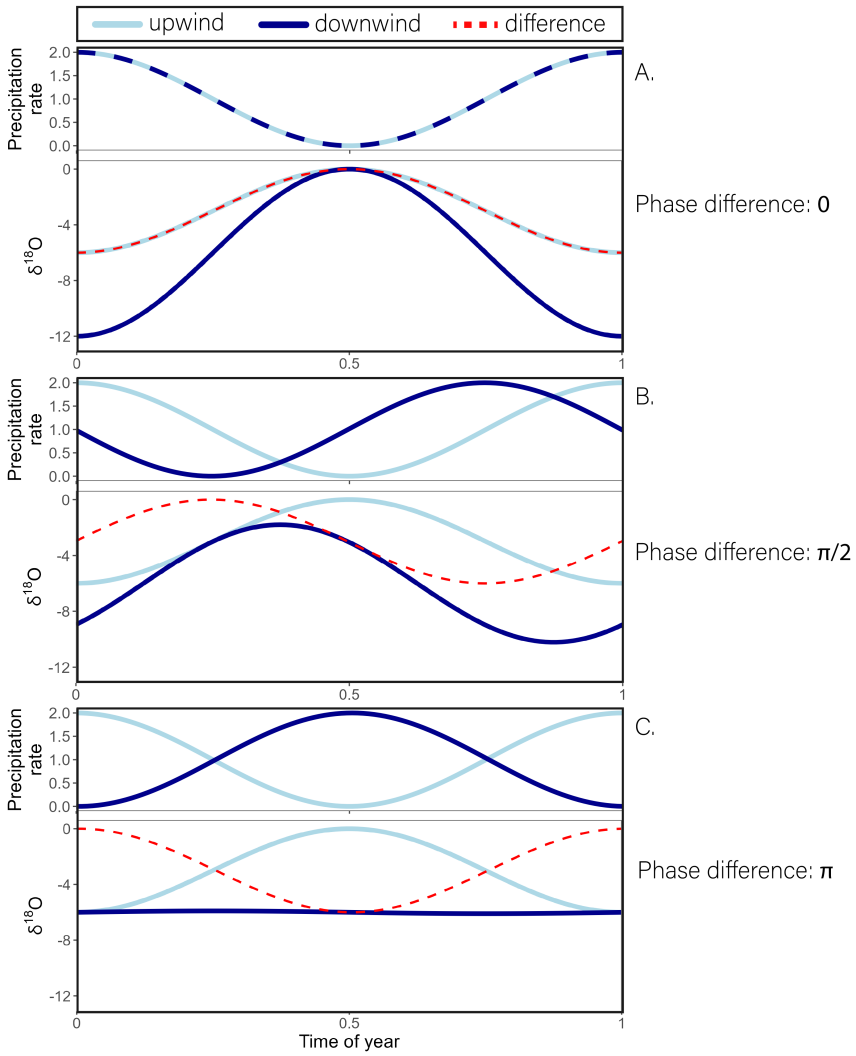

Figure S11. Precipitation and $\delta^{18}O$ for three phase differences. Results from the toy model for precipitation seasonality. Each panel (A-C) shows the annual cycle of the precipitation rate at each site (top; light blue is upwind, dark blue is downwind), and the annual cycle of $\delta^{18}O$ at each sites, as well as $\Delta\delta^{18}O$ (bottom; $\Delta\delta^{18}O$ is red dashed line). Panel (**A**) is a phase difference of zero; Panel (**B**) is a phase difference of $\frac{\pi}{2}$, or 3 months, and Panel (**C**) is a phase difference of π, or 6 months.

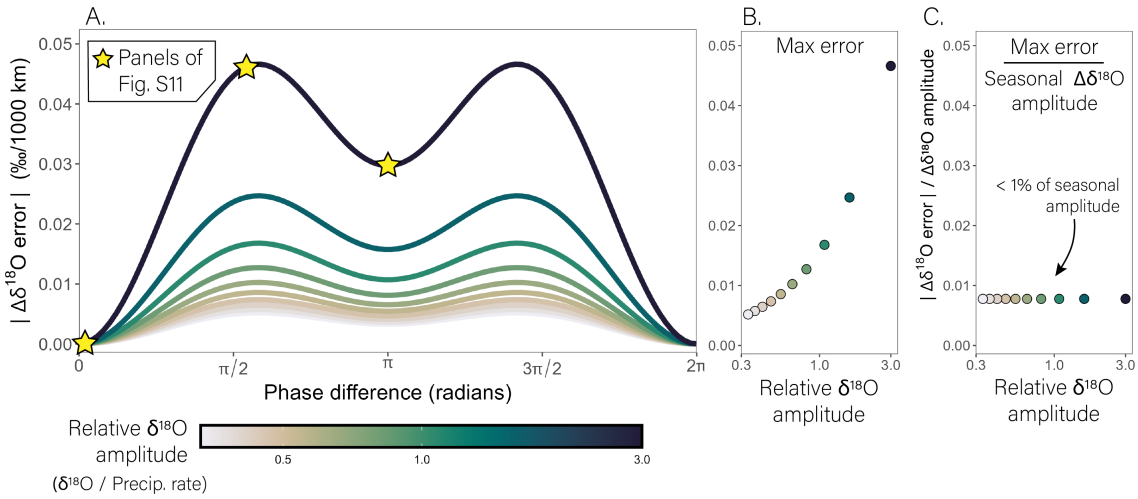

Figure S12. Sensitivity of $\Delta\delta^{18}O$ to differences in the phase of precipitation seasonality between sites. Stars denote panels in Figure S11. (**A**) Absolute $\Delta\delta^{18}O$ error (relative to no phase difference) for a phase difference of zero to 12 months (0 to 2π). Colored lines show different sensitivities of $\delta^{18}O$ to precipitation (relative $\delta^{18}O$ amplitudes). (**B**) The maximum $\Delta\delta^{18}O$ error for each relative $\delta^{18}O$ amplitude. (**C**) Maximum $\Delta\delta^{18}O$ error divided by the seasonal amplitude of $\Delta\delta^{18}O$. Relative to the seasonal $\Delta\delta^{18}O$ amplitude, the error induced by phase differences between sites is less than 1%.